Thermochimica Acta 509 (2010) 62–66

Contents lists available at ScienceDirect

Thermochimica Acta

journal homepage: www.elsevier.com/locate/tca

A DSC study of the $NaNO_3$–KNO_3 system using an innovative encapsulation technique

O. Beneš*, R.J.M. Konings, S. Wurzer, M. Sierig, A. Dockendorf

European Commission, Joint Research Centre, Institute for Transuranium Elements, P.O. Box 2340, 76125 Karlsruhe, Germany

ARTICLE INFO

Article history:
Received 13 April 2010
Received in revised form 28 May 2010
Accepted 2 June 2010
Available online 11 June 2010

Keywords:
Phase diagram
DSC
Encapsulation
Alkali nitrates

ABSTRACT

An innovative encapsulation technique designed for the DSC high temperature measurements of the volatile samples is presented in this study. Stainless steel crucibles with a screwed bolt were developed for this purpose. The technique was demonstrated on the phase diagram measurement of the $NaNO_3$–KNO_3 system and the obtained results are presented in this study. Up to date two thermodynamic assessments of the $NaNO_3$–KNO_3 phase diagram have been made, one characterized by a single eutectic point with limited solubilities in the solid state in both $NaNO_3$ and KNO_3 rich corners, whereas the other version prefers a continuous solid solubility with minimum on the liquidus line. Based on our results we confirm limited solubilities in the solid state.

1. Introduction

In order to avoid vaporization of volatile samples during high temperature differential scanning calorimetry (DSC) measurements it is necessary to encapsulate them and maintain them closed at operating temperatures. This is important for a phase diagram study since a composition shift can be caused by an incongruent vaporization bringing an error to the measurement. In case of measuring samples that act corrosively (e.g. alkali fluorides) the encapsulation is the only safe way to avoid the risk of damage of the detector. For these two reasons we have developed an encapsulation technique that is compatible with the DSC sensor of the Setaram multi detector high temperature calorimeter (SETARAM MDHTC96) which is used to perform our experiments. The main objective was to make a design that would be compatible with the molten fluoride salts which are the prime candidates as a molten salt reactor fuel. However since the fluorides are corrosive against the platinum used as a main material in the sensor's thermocouples this novel technique was first demonstrated on the measurement of the $NaNO_3$–KNO_3 phase diagram. This system is considered as one of the possible choices for a heat transfer salt for the Generation IV nuclear reactors so its melting knowledge is of great importance. The study of this phase diagram is considered as an ideal test for our new technique since the nitrates melt relatively low so a re-opening (as discussed in Section 2) of the crucibles was possible after every heat treatment and it was also safe to take the risk of possible leakage since the nitrates are not corrosive against platinum at the measured temperatures. Furthermore the alkali nitrates have significant vapour pressure above their melting points so it was easy to check the gas tightness using a simple mass balance of the crucible performed before and after the measurement.

According to literature two thermodynamic assessments of the $NaNO_3$–KNO_3 phase diagram have been made. One suggesting continuous solid solution of the rhombohedral crystal structure [1] whereas a more recent study [2] indicates an eutectic system with a limited solubility in the solid state at both $NaNO_3$ and KNO_3 corners. Both versions of the $NaNO_3$–KNO_3 phase diagrams are discussed in Section 4 and a new thermodynamic assessment based on our DSC data is presented.

2. Encapsulation technique

In order to make a design of the sample encapsulation compatible with the used DSC sensor several requirements had to be fulfilled. The first one is related to the dimensions which had to be such that the crucible perfectly fits into the sample compartment of the SETARAM MDHTC96 DSC detector in order to keep a good thermal contact. It is also required that the crucible is firm enough to hold the overpressure caused by a gas thermal expansion or/and by a vaporization of the measured sample up to 1673 K (maximal operating temperature of the used DSC). Moreover the crucible must be strong enough not to deform due to this overpressure because even a slight deformation could damage the fragile detector (alumina tube) since the gap between the crucible and the detector tube is minimal. Furthermore it is important that the crucible is a good

* Corresponding author. Tel.: +49 7247 951 385; fax: +49 7247 951 99385.
E-mail address: ondrej.benes@ec.europa.eu (O. Beneš).

0040-6031/$ – see front matter © 2010 Elsevier B.V. All rights reserved.
doi:10.1016/j.tca.2010.06.003

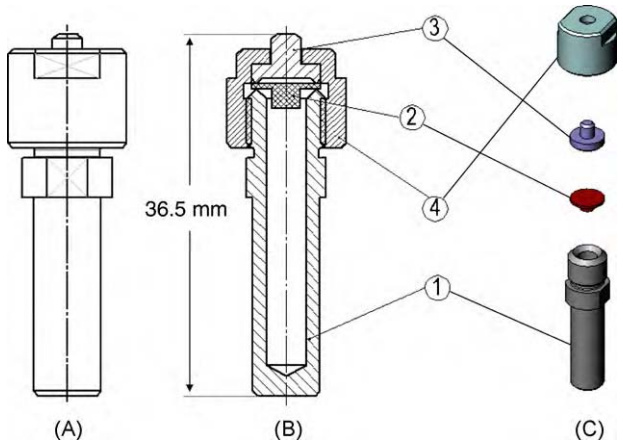

Fig. 1. Schematic representation of the DSC crucible developed for fluoride samples measurements. (A) A scheme of the side of the developed DSC crucible; (B) a scheme of a cut of the crucible; (C) various parts of a crucible: 1, stainless steel crucible, 2, nickel sealing, 3, stainless steel stopper, and 4, stainless steel closing bolt.

Fig. 2. Left: a stainless steel crucible developed for the DSC measurements of volatile samples; right: boron nitride liner which is inserted into the crucible to separate the sample and the main body of the crucible.

thermal conductor so a good DSC signal between the sample and the detector is maintained.

As a material that is easily available and fulfills the above mentioned criteria a stainless steel was proposed. In order to avoid its oxidation at high temperatures all measurements must be performed at constant flow of inert gas. For all experiments performed in this study the high purity (6.0 grade) argon gas was used. A scheme of a prototype of the developed DSC crucible is shown in Fig. 1. It consists of four parts; the main body of the crucible which is made of stainless steel (1.4301 type) with the wall thickness of 1.4 mm, strong enough to keep its shape at high temperature; of a nickel ring which, due to its softness, serves as a sealing and is squeezed between the main body and the stainless steel stopper by a bolt which is stainless steel as well. In order to achieve absolute tightness the stopper and the main body have a sharp edge which is in tight contact with the sealing.

Furthermore the design had to enable to re-use the crucible after the measurement. However this option has been fulfilled only in case of the measurement of the $NaNO_3$–KNO_3 phase diagram due to the relatively low melting temperature of nitrates on one hand side and a good solubility of nitrates in water on the other hand so perfect clean-up of the used crucible could be performed after each measurement. This is unfortunately not the case for fluoride samples which in general melt at higher temperatures, so the opening of the crucibles after the high temperature treatment was more difficult due to the steel sintering on the screws.

Finally it was necessary to design the crucible in such a way that it would be compatible with the fluoride samples at elevated temperatures.

Since the proposed crucible is made from a stainless steel that is corroded by fluorides at high temperatures a boron nitride (AX-05 grade) liner has been inserted into the main body of the crucible in order to separate the sample and the inner walls. The dimensions of the liner are such that it perfectly fits into the crucible so a good thermal contact remains while the top edge of the liner touches the nickel sealing in order to minimize a contact of the sample vapour with the stainless steel. Since the crucibles are developed for the measurements of molten fluoride salts this option was shown as very important as fluorides do not react with boron nitride neither do they with pure nickel. It is shown in Fig. 1 that the nickel sealing is not a simple plate but it consists of an additional cylindrical part of a smaller diameter which exactly fits into the boron nitride liner and keeps its position during the closing procedure of the whole crucible. It sometimes appeared that when only a simple plate was used it slightly moved during the closing procedure resulting into a leakage.

Both, liner and the crucible, are shown in Fig. 2. Boron nitride has been found as an ideal material as it is easily available, relatively cheap, it is highly thermally conductive and it is non-reactive with fluorides.

To avoid the need of the boron nitride liner it was first proposed to make a crucible from pure nickel, because nickel is a good thermal conductor and it is also compatible with the fluorides even at very high temperatures, however this material is too soft so the strength criterions could not be achieved. Another solution was to make it from nickel based alloys like Hastelloy-N used in the Molten Salt Breeder Reactor project or from MoNiCr alloy which would fulfill all three technical requirements, however the price of a crucible made from these materials would be much higher so that the stainless steel option with the boron nitride liner has been proposed as in case of fluoride sample measurements it has only a single use.

3. $NaNO_3$–KNO_3 phase diagram study

The first system that has been investigated using our novel encapsulation technique was the $NaNO_3$–KNO_3 binary system.

Pure $NaNO_3$ and KNO_3 compounds, both from Alfa Aesar of 99.999 and 99.994 wt.% metal purity respectively, have been used as starting materials. Their melting temperatures have been measured as well and a very good agreement to the literature data [3] has been found. In case of pure $NaNO_3$ the observed melting temperature was $T_{melting}$ = 579.6 K compared to 579 K from [3] and in case of pure KNO_3 the measured melting point was $T_{melting}$ = 606.8 K whereas a value of 606 K is reported in [3].

The mixtures have been prepared by direct mixing in the crucibles to achieve minimal composition errors. After the crucibles were closed they were inserted into the calorimeter and measured. All measurements were performed using the Setaram MDHTC with installed DSC detector (S-type thermocouple). For each composition three heating and cooling runs have been made in total. The first cycle has been made to achieve perfect mixing of the precursors and the results from this sequence have never been taken into account. The other two cycles have been analyzed and the data from these runs are reported in Table 1. A typical DSC heating curve for pure KNO_3 and $Na_{0.347}K_{0.653}NO_3$ mixture is shown in Figs. 3 and 4

Table 1
Transition temperature data of the $NaNO_3$–KNO_3 system obtained by DSC in this study.

X_{KNO_3}	T (K)	Transition	X_{KNO_3}	T (K)	Transition
0	579.6	Melting	0.481	496.4	Solidus
0	545.5	Transition	0.481	496.4	Liquidus
0.027	574.7	Liquidus	0.499	383.3	Eutectoid
0.038	573.2	Liquidus	0.499	496.9	Solidus
0.069	383	Eutectoid	0.549	384.7	Eutectoid
0.069	576.9	Liquidus	0.549	496.9	Solidus
0.096	384	Eutectoid	0.600	497.4	Solidus
0.096	503.5	Solidus	0.600	514.8	Liquidus
0.096	574.1	Liquidus	0.653	382.7	Eutectoid
0.103	384.9	Eutectoid	0.653	497.6	Solidus
0.103	501.2	Solidus	0.653	526	Liquidus
0.103	572.2	Liquidus	0.697	383.2	Eutectoid
0.143	383.6	Eutectoid	0.697	486.2	Solidus
0.143	498.8	Solidus	0.697	534.4	Liquidus
0.143	568	Liquidus	0.751	383.1	Eutectoid
0.203	384.1	Eutectoid	0.801	384.1	Eutectoid
0.203	496	Solidus	0.801	498.8	Solidus
0.203	562.8	Liquidus	0.801	567.4	Liquidus
0.257	384.8	Eutectoid	0.818	384	Eutectoid
0.257	497.4	Solidus	0.818	496.5	Solidus
0.257	554.2	Liquidus	0.818	575.4	Liquidus
0.313	383.6	Eutectoid	0.85	383.9	Eutectoid
0.313	496	Solidus	0.85	500.3	Solidus
0.313	532.1	Liquidus	0.85	579.8	Liquidus
0.345	385.3	Eutectoid	0.877	383.5	Eutectoid
0.345	497.1	Solidus	0.877	535.5	Solidus
0.345	522.6	Liquidus	0.877	581.5	Liquidus
0.36	386.1	Eutectoid	0.899	383.4	Eutectoid
0.36	497	Solidus	0.899	551.1	Solidus
0.36	523	Liquidus	0.899	590.6	Liquidus
0.425	384.5	Eutectoid	0.949	384.4	Eutectoid
0.425	496.9	Solidus	0.949	563.8	Solidus
0.425	509.2	Liquidus	0.949	602.9	Liquidus
0.46	381.7	Eutectoid	1	405.6	Transition
0.46	494.1	Solidus	1	606.8	Melting
0.46	508.2	Liquidus			
0.481	383.6	Eutectoid			

respectively. The two figures also show the tangential analysis of the recorded heat flow (DSC signal) peaks which is recommended for the thermal analysis measurements. The temperature range of all experiments was 293–673 K, thus the maximum temperature was always higher than the melting temperature of pure KNO_3, the higher melting end-member. The heating rates were 3 and 5 K/min and from both measurements nearly identical results have been obtained. The measured values were corrected with the calibration curve that was obtained from the measurements of pure standard

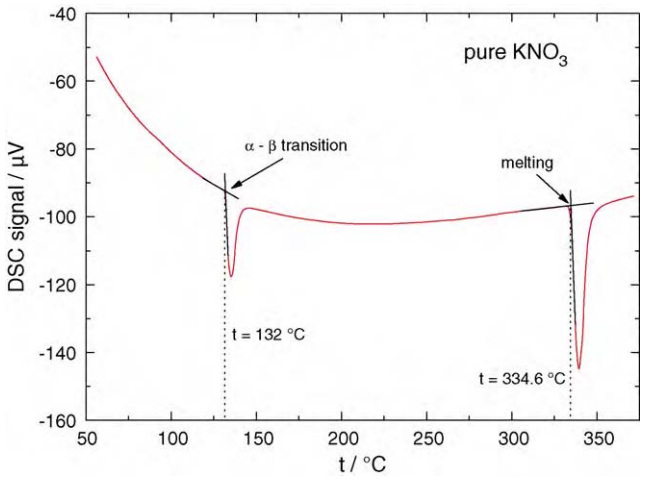

Fig. 3. DSC analysis of the measurement of pure KNO_3.

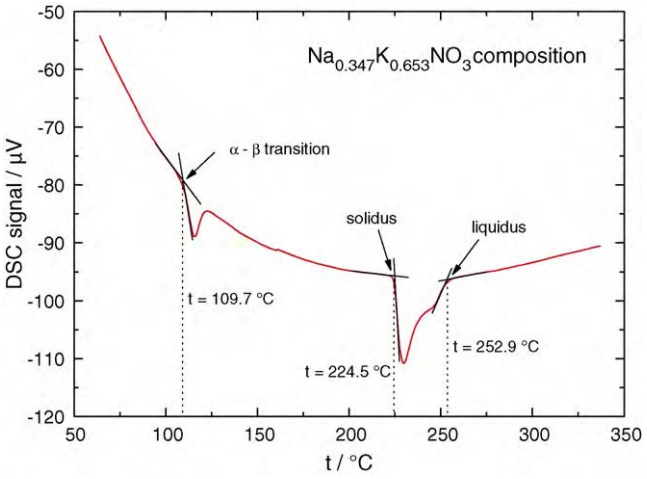

Fig. 4. DSC analysis of the measurement of the $Na_{0.347}K_{0.653}NO_3$ composition.

metals (In, Sn, Zn, Pb, Al, Ag and Au) of various melting temperatures in order to cover the temperature range of the calorimeter. Due to the supercooling effect of the nitrate salts the results from the cooling sequences have never been taken into account.

As reported in Table 1 two invariant equilibria were measured in the $NaNO_3$–KNO_3 system, the eutectoid assigned with the KNO_3 solid–solid transition and the eutectic. The measured eutectoid temperature was determined as an average temperature of all eutectoid values from Table 1, thus $T_{eutectoid} = 383.9 \pm 0.9$ K. The same approach was used to derive the eutectic temperature taking it as an average value of the solidus points measured between the composition range $X(KNO_3) = 0.15$–0.85, thus $T_{eutectic} = 496.5 \pm 3$ K. Corresponding eutectic composition was determined based on the half-width of the DSC peak indicating $X_{eutectic}(KNO_3) = 0.51 \pm 0.02$.

4. Discussion about the $NaNO_3$–KNO_3 phase diagram

As discussed previously the main objective of this study was to develop and test an encapsulation technique for the DSC measurements which will be used in the future for experiments with the fluoride salts. For various reasons as specified in Section 1 the first system to be studied using our novel technique was the $NaNO_3$–KNO_3 system. As summarized in [1] several measurements have been performed to describe the $NaNO_3$–KNO_3 phase diagram [4–34]. All results from these reports have been plotted in one figure in [1] which we refer to for details. As mentioned in Section 1 based on these experimental results two different phase diagrams were suggested, one with continuous solution in the solid state, whereas the other one favors only limited solubilities at $NaNO_3$ and KNO_3 rich sides. The new experimental data obtained in this study confirm limited solubilities in the solid state since nearly constant values on the solidus line have been found for wide composition range, $X(KNO_3) = 0.15$–0.85 as shown in Fig. 5. This observation is also supported by the high temperature X-ray analysis of the $NaNO_3$–KNO_3 (1:1) mixture reported by Zhang et al. [2] few degrees below the solidus at $T = 473$ K. They clearly found two different phases on their diffractogram, one assigned to $NaNO_3$ phase while the other one to the KNO_3 phase. Moreover as discussed by the same authors the continuous solid solution model is not consistent with the Raman studies performed by Xu and Chen [35,36]. They first measured the temperature dependence of the Raman spectra of different compositions of the $NaNO_3$–KNO_3 mixture and from the obtained results concluded that the $NaNO_3$–KNO_3 system might be regarded as a system with limited solid solutions instead of continuous one. This observation was later confirmed by the same group

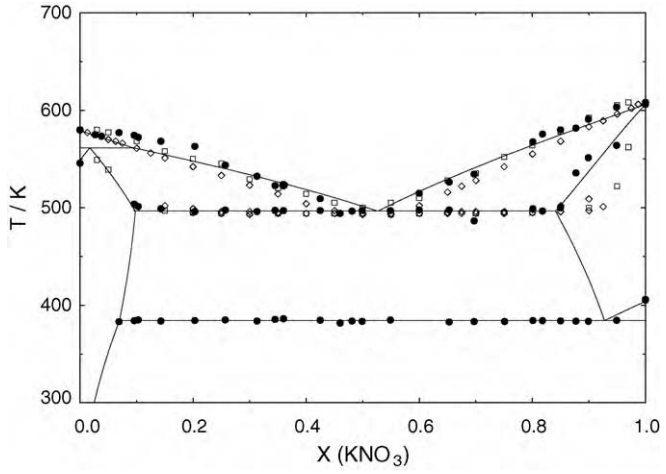

Fig. 5. The optimized $NaNO_3$–KNO_3 phase diagram, (●) DSC data obtained in this study, (□) DSC data obtained by Kramer and Wilson [28], and (◊) DSC data obtained by Greis et al. [31].

by measuring the Raman spectra of the quenched samples. In the study by Berg and Kerridge [37] an additional evidence from Raman spectroscopy and Raman mapping of the $NaNO_3$–KNO_3 (1:1) composition has been presented, supporting the eutectic composition with the solid state transition at around 388 K attributed to the phase transition in KNO_3 rich area.

Based on the strong experimental evidence of the two-phase region below the solidus line the $NaNO_3$–KNO_3 phase diagram has been re-assessed using the experimental data measured in this study. The same phase diagram with limited solubilities in the solid state has been modelled in a work by Zhang et al. [2], however these authors did not consider the α–β phase transitions of the $NaNO_3$ and KNO_3 end-members which must be included in the phase diagram description. As a consequence of the KNO_3 phase transition an eutectoid appears in this system which has been clearly observed from the DSC measurements made in this work. The eutectoid transition was also observed by Zhang et al. as shown in their DSC profile, but was not taken into account in their phase diagram assessment.

5. Thermodynamic assessment of the $NaNO_3$–KNO_3 system

Using the equilibrium data obtained in this study the $NaNO_3$–KNO_3 phase diagram has been thermodynamically re-assessed assuming limited solubilities in the solid state at $NaNO_3$ and KNO_3 corners. All thermodynamic calculations performed in this study were done using the FactSage software [38] based on the Gibbs energy minimization. For the description of the excess Gibbs parameters of both binary liquid and solid solutions a simple polynomial formalism has been used. The total Gibbs energy of such solution is given by the following equation:

$$G(T) = X_{NaNO_3} \cdot G^{\circ}_{m,NaNO_3}(T) + X_{KNO_3} \cdot G^{\circ}_{m,KNO_3}(T) + X_{NaNO_3} RT \ \ln X_{NaNO_3} + X_{KNO_3} RT \ln X_{KNO_3} + G^{xs}_m \quad (1)$$

where G°_m is the molar standard Gibbs energy of pure end-members,

$$G^{xs}_m = \sum_{i,j} X_{NaNO_3} \cdot X_{KNO_3} \cdot L_{i,j} \quad (2)$$

and X_{NaNO_3} and X_{KNO_3} are the mole fractions of $NaNO_3$ and KNO_3 respectively. The $L_{i,j}$ term from Eq. (2) is the general polynomial equation:

$$L_{i,j} = a + bT + cT \ln T + dT^2 + \ldots. \quad (3)$$

with parameters to be optimized during the thermodynamic assessment.

Two solid solutions occur in the $NaNO_3$–KNO_3 system. The $NaNO_3$-rich solid phase was treated as a mixture of α-$NaNO_3$ and α-KNO_3 and is described by the following formula:

$$G^{xs}_{NaNO_3\text{-rich}}(\mathrm{J\,mol^{-1}}) = X_{KNO_3} RT \ln \gamma_{KNO_3} = (11{,}580 - 8T) X_{KNO_3} \quad (4)$$

For the reasons of the same crystallographic structures of the β phases of both end-members the KNO_3 rich solid solution was treated as a mixture of β-$NaNO_3$ and β-KNO_3 and the optimized excess Gibbs function of this solution obtained in this study is given below:

$$G^{xs}_{KNO_3\text{-rich}}(\mathrm{J\,mol^{-1}}) = X_{NaNO_3} RT \ln \gamma_{NaNO_3} = (8800 - 4T) X_{NaNO_3} \quad (5)$$

The optimization of the excess Gibbs function of the $Na_{1-x}K_xNO_3$ liquid solution was based on the mixing enthalpies experimentally determined by Kleppa [39] for a temperature range between 619 K and 723 K. Based on these data he derived the temperature independent mixing enthalpy as a function of composition as:

$$H^{xs}_{liquid}(\mathrm{J\,mol^{-1}}) = X_{NaNO_3} \cdot X_{KNO_3}(-1709.2 - 274.5 \cdot X_{NaNO_3}) \quad (6)$$

This equation was also used in this study, but for the description of the excess Gibbs energy a small temperature dependent parameter was added in order to better fit the experimental results from this study. The full optimized excess Gibbs energy of the $(Na_{1-x},K_x)NO_3$ liquid solution obtained in our assessment is given below:

$$G^{xs}_{liquid}(\mathrm{J\,mol^{-1}}) = X_{NaNo_3} \cdot X_{KNo_3}(-1709.2 + 5.2T - 284.5 \cdot X_{NaNo_3}) \quad (7)$$

The thermodynamic data of pure solid and liquid phases of the $NaNO_3$ and KNO_3 compounds used in the thermodynamic evaluation are summarized in Table 2. The temperature functions of the

Table 2
The thermodynamic data of the $NaNO_3$ and KNO_3 pure phases used in this study.

Compound	$\Delta_f H^0_{(298.15)}$ (kJ mol^{-1})	$S^0_{(298.15)}$ (J K^{-1} mol^{-1})	$C_p = a + bT + cT^2$		
			a	bT	cT^2
α-$NaNO_3$	−467.700	116.300	22.62	0.222	
β-$NaNO_3$	−469.686	107.532	139.0		
$NaNO_3$(l)	−454.481	133.935	138.2		
α-KNO_3	−494.630	133.000	37.49	0.191	
β-KNO_3	−492.642	136.451	255	−0.569	6.310^{-4}
KNO_3(l)	−486.076	145.141	142.7		

Table 3
Melting temperatures of pure alkali fluorides measured in this study.

Compound	$T_{experimental}$ (K)	$T_{literature}$ (K)
LiF	1120.0	1121 ± 1 [41]
NaF	1268.6	1269 ± 2 [41]
KF	1120.5	1131 [41]
RbF	1060.9	1068 [40]

heat capacity of all presented phases were taken from Jriri et al. [3] while the absolute entropy of α-KNO_3 and α-$NaNO_3$ at 298.15 K were taken from Carling [30]. The reference enthalpies for the α-KNO_3 and α-$NaNO_3$ phases at 298.15 K were taken from Glushko thermodynamic tables [40] whereas the reference enthalpies and the absolute entropies at 298.15 K for the higher temperature phases (β-phase, liquid phase) were derived based on the transition temperatures and transition heats taken from [3].

The optimized $NaNO_3$–KNO_3 phase diagram together with the DSC data obtained in this study is shown in Fig. 5. A comparison to the data measured in [28,31] using a DSC technique is reported in the figure as well showing a good correlation. As discussed in Section 4 this system consists of a simple eutectic with limited solubilities in the solid state at $NaNO_3$ and KNO_3 rich sides. The calculated eutectic was found at $T = 496$ K and $X_{KNO_3} = 0.53$ in perfect agreement to our experimental data, whereas the maximum solubilities of the $NaNO_3$ and KNO_3 solid solutions were found at the eutectic temperature and $X_{KNO_3} = 0.10$ and $X_{KNO_3} = 0.84$ respectively. The eutectoid temperature was calculated at $T = 384$ K and $X_{KNO_3} = 0.93$ with a very good agreement to the measurements as well.

6. Conclusions

A novel encapsulation technique for the DSC measurements was developed. It has been demonstrated on the $NaNO_3$–KNO_3 series of measurements that the developed crucibles are a very promising solution to encapsulate volatile samples while keeping a DSC signal strong enough to identify the equilibrium points. New equilibrium data of the $NaNO_3$–KNO_3 phase diagram were presented indicating a single eutectic system with a limited solubility in the solid state at both $NaNO_3$ and KNO_3 sides. Based on the obtained results the phase diagram was re-evaluated and the optimized excess Gibbs parameters were presented.

To demonstrate the applicability of these crucibles for the measurements of the fluoride salts we have determined melting temperatures of pure LiF, NaF, KF and RbF compounds which were compared to the literature values as shown in Table 3 and a very good agreement is evident. Since no deformation, leakage or corrosion was observed during the performed experiments this technique is now envisioned for the future measurements of the fluoride salts.

References

[1] T. Jriri, J. Rogez, J.C. Mathieu, I. Ansara, J. Phase Equilibr. 20 (1999) 515–525.
[2] X. Zhang, J. Tian, K. Xu, Y. Gao, J. Phase Equilibr. 24 (2003) 441–446.
[3] T. Jriri, J. Rogez, C. Bergman, J.C. Mathieu, Thermochim. Acta 266 (1995) 147–161.
[4] F.G. Schaffgotsch, Ann. Phys. Chem. 102 (1857) 293–299.
[5] F. Guthrie, Philos. Mag. 17 (1884) 462–482.
[6] H.R. Carveth, J. Phys. Chem. 2 (1898) 209–226.
[7] D.J. Hissink, J. Phys. Chem. 32 (1900) 537–563.
[8] A.W.C. Menzies, N.N. Dutt, J. Am. Chem. Soc. 33 (1911) 1366–1375.
[9] M. Amadori, Atti. Ist. Veneto Sci., Lett. Arti, Cl. Sci. Mater. Nat. 72 (1912) 451–460.
[10] W.D. Harkins, G.L. Clark, J. Am. Chem. Soc. 37 (1915) 1816–1828.
[11] A. Quartaroli, Gazz. Chim. Ital. 50 (1920) 64–69.
[12] H.V.A. Briscoe, W.M. Madgin, J. Chem. Soc. Lond. 123 (1923) 1608–1618.
[13] W.H. Madgin, H.V.A. Briscoe, J. Chem. Soc. 123 (1923) 2914–2916.
[14] K. Laybourn, W.M. Madgin, J. Chem. Soc. Lond. 874 (1932) 2582–2589.
[15] A.G. Bergmann, N.M. Vaksberg, Izv. Akad. Nauk SSSR, Otd. Matem. Estest. Nauk 1 (1937) 71–95.
[16] F.I. Vasenin, A.G. Bergman, Izv. Sekt. Fiz. Khim. Anal. 11 (1938) 169–187.
[17] E. Jänecke, Z. Elektrochem, Angew. Phys. Chem. 48 (1942) 453–512.
[18] M.I. Ravich, F.B. Ginzburg, Izv. Akad. Nauk SSSR Otd. Khim. Nauk 2 (1947) 141–151.
[19] A.G. Bergmann, N.M. Vaksberg, Izv. Sekt. Fiz. Khim. Anal. 16 (1948) 66–81.
[20] P.I. Protsenko, A.G. Bergman, Zh. Obshch. Khim. 20 (1950) 1365–1375.
[21] A.G. Bergmann, S.I. Beruly, Anal. Inst. Obshch. Neorg. Khim. Akad. Nauk SSSR 21 (1952) 178–183.
[22] S.I. Beruly, A.G. Bergmann, Anal. Inst. Obshch. Neorg. Khim. Akad. Nauk SSSR 25 (1954) 218–235.
[23] A. Kofler, Montash. Chem. 86 (1955) 643–652.
[24] B.S. Brcic, L.G. Golic, J. Jernejcic, P. Zemva, Monatsh. Chem. 93 (1962) 1243–1253.
[25] M.P. Susarov, A.I. Efimov, L.S. Timoshenko, Russ. J. Phys. Chem. 43 (1969) 795–799.
[26] W. Klement, J. Inorg. Nucl. Chem. 36 (1974) 1916–1918.
[27] R. Vilcu, F. Irinei, E. Tatu, Rev. Roum. Chim. 121 (1976) 491–494.
[28] C.M. Kramer, C.J. Wilson, Thermochim. Acta 42 (1980) 253–264.
[29] D.J. Rogers, G.J. Janz, J. Chem. Eng. Data 27 (1982) 424–428.
[30] R.W. Carling, Thermochim. Acta 60 (1983) 265–275.
[31] O. Greis, K.M. Bahamdan, B.M. Uwais, Thermochim. Acta 86 (1985) 343–350.
[32] H.G. Wiedmann, G. Bayer, J. Therm. Anal. 30 (1985) 1273–1281.
[33] Y.E. Baktinov, S.E. Darienko, Y.F. Chervinskii, Zh. Neorg. Khim. 36 (1991) 2915–2918.
[34] H. Zamali, M.J. Jemal, J. Therm. Anal. 41 (1994) 1091–1099.
[35] K.C. Xu, Y. Chen, J. Raman Spectrosc. 30 (1999) 173–179.
[36] K.C. Xu, Y. Chen, J. Raman Spectrosc. 30 (1999) 441–448.
[37] R.W. Berg, D.H. Kerridge, Dalton Trans. (2004) 2224–2229.
[38] C. W. Bale, et al., FactSage Software, v 5.5.
[39] O.J. Kleppa, J. Phys. Chem. 64 (1960) 1937–1940.
[40] V. P. Glushko, et al., Glushko Thermocenter of the Russian Academy of Sciences, IVTAN Association, Izhorskaya 13/19, 127412 Moscow, Russia.
[41] M.W. Chase Jr. (Ed.), NIST-JANAF Thermochemical Tables Fourth Edition, Part II, Cr–Zr. J. Phys. Chem. Ref. Data, Monogr. 9 (1998).